

Tracing the phase of focused broadband laser pulses

Dominik Hoff,^{1,*} Michael Krüger,^{2,3,*} Lothar Maisenbacher,⁴
A. M. Saylor,¹ Gerhard G. Paulus,¹ and Peter Hommelhoff^{2,4,5}

¹*Helmholtz-Institut Jena and Institut für Optik und Quantenelektronik,
Friedrich-Schiller-Universität Jena, Max-Wien-Platz 1, D-07743 Jena, Germany*

²*Department Physik, Friedrich-Alexander-Universität Erlangen-Nürnberg (FAU), Staudtstr. 1, D-91058 Erlangen, Germany*

³*Department of Physics of Complex Systems, Weizmann Institute of Science, 234 Herzl St., Rehovot 76100, Israel*

⁴*Max-Planck-Institut für Quantenoptik, Hans-Kopfermann-Str. 1, D-85748 Garching, Germany*

⁵*Max-Planck-Institut für die Physik des Lichts, Staudtstr. 2, D-91058 Erlangen, Germany*

The corresponding Nature Physics paper and the supplementary material is available at <http://dx.doi.org/10.1038/nphys4185>.

Precise knowledge of the behaviour of the phase of light in a focused beam is fundamental to understanding and controlling laser-driven processes. More than a hundred years ago an axial phase anomaly for focused monochromatic light beams was discovered and is now commonly known as the Gouy phase¹⁻⁴. Recent theoretical work has brought into question the validity of applying this *monochromatic* phase formulation to the broadband pulses becoming ubiquitous today^{5,6}. Based on electron back-scattering at sharp nanometre-scale metal tips, a method is available to measure light fields with sub-wavelength spatial resolution and sub-optical cycle time resolution⁷⁻⁹. Here we report such a direct, three-dimensional measurement of the spatial dependence of the optical phase of a focused, 4-fs, near-infrared laser pulse. The observed optical phase deviates substantially from the monochromatic Gouy phase — exhibiting a much more complex spatial dependence, both along the propagation axis and in the radial direction. In our measurements, these significant deviations are the rule and not the exception for focused, broadband laser pulses. Therefore, we expect wide ramifications for all broadband laser-matter interactions, such as in high-harmonic and attosecond pulse generation, femtochemistry¹⁰, ophthalmological optical coherence tomography^{11,12} and light-wave electronics¹³.

In ultrafast light-matter interactions, the phase of the optical carrier field with respect to the pulse envelope's maximum — the carrier-envelope phase (CEP, see Methods)¹⁴ — is one of the fundamental controls that allows one to steer chemical reactions¹⁵, the generation of attosecond pulses via high-harmonic generation¹⁶, and electron emission and acceleration from solid surfaces and nanostructures^{7,9,17}, among others. Hence, determining and controlling the CEP is mandatory in many fields using lasers, but taking into account the broadband and often intense and ultrashort nature of these pulses is challenging and an active area of research^{18,19}. Further, non-

linear light-matter interactions usually take place in the focus of a beam where the CEP shows a strong spatial dependence. Thus, for a detailed understanding of and field control over these processes, it is essential to take the focal phase evolution, target position, and target extent into account^{13,20}. This is as important as controlling the CEP of the input beam itself.

For a focused monochromatic beam, the on-axis phase shift due to diffraction is described by the familiar Gouy phase, which follows a simple arctangent curve^{1,2}. However, many of today's coherent light sources, even some as common place as those used in ophthalmological diagnostics, are far from being monochromatic. Rather, they can span close to, and many even exceed, an octave of spectral bandwidth^{12,21,22}. Further, recent theoretical studies, based on diffraction theory for pulsed Gaussian beams, yielded spatially-dependent phases that significantly deviate from the simple Gouy phase and show a much more complex behaviour that is dictated by the wavelength-dependent input beam geometry^{5,6}. The need for further investigation is underscored by experimental studies, which strongly suggest deviations from the monochromatic Gouy phase²³⁻²⁵.

In recent years, significant advancements have been made in CEP detection and control^{14,16,18,26}, which have facilitated and driven the discovery of more and more processes that are dependent on and can be controlled via the CEP. One such phenomenon is the strong-field, few-cycle-laser-driven back-scattering of photoelectrons, i.e. those electrons freed by the laser field that can then be driven back to and scattered off their parent matter when the field flips sign within an optical cycle. The large kinetic energy obtained by these electrons strongly depends on the CEP, which we utilize as an experimental signature, see Supplementary information. This extremely CEP-sensitive effect was observed in noble gases and recently also at solid state nanotips⁷⁻⁹. For the latter, strong-field induced photo-emission happens almost exclusively in the enhanced optical near-field region at the apex of the sharp tip, with a radius of ~ 10 nm²⁷. Thus, electrons from such a highly-localized source are particularly well suited to be used as a sensor to probe focused light fields with resolution better than their natural length and time scales. Namely here, with a spatial resolution of ~ 10 nm ($\ll \lambda/2 \approx 350$ nm, the typical length scale of a focus of light with wavelength of $\lambda \approx 700$ nm),

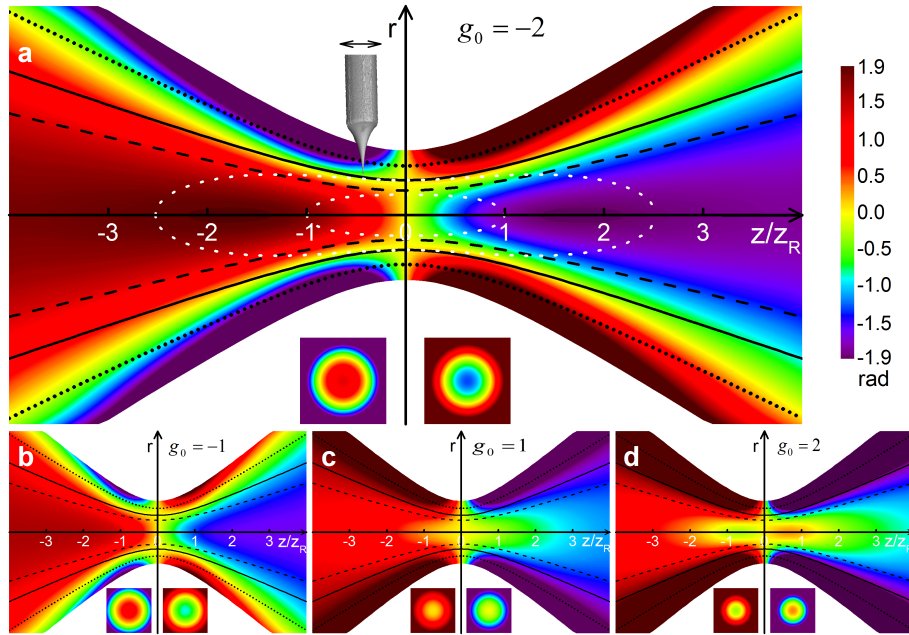


FIG. 1. **Carrier-envelope phase in a focused, broadband, pulsed Gaussian beam.** The colour plots show the calculated CEP in the focus of an input beam with geometry factors of (a) $g_0 = -2$, (b) $g_0 = -1$, i.e. isodivergent, (c) $g_0 = 1$, which has a wavelength independent beam waist, and (d) $g_0 = 2$ as a function of axial and radial position, z and r respectively. The factor g_0 is explained in the text and describes the spectral input beam geometry. For visual convenience, the colour is truncated for $|\Delta\phi| > 1.9$ rad and the beam size at $r > 1.86 w(z)$ where the intensity has dropped below a factor of 10^{-3} of the on-axis value. Cross sections in the x - y -plane are given for an alternative perspective of the same data at $z = -0.5$ and $0.5 z_R$ in the same radius range (insets). The black lines are hyperbolae related to the local $1/e^2$ intensity radius $w(z)$, namely at $r = w(z)/\sqrt{2}$ (dashed), $r = w(z)$ (solid), $r = \sqrt{2} w(z)$ (dotted). The white dotted lines are isointensity curves of $I_0/2$ and I_0/e^2 (see Supplementary information). The CEP is probed by recording photoelectron spectra with a metal nanotip (drawn to scale) on the optical axis and on the hyperbolae in the half space towards the tip. In the measurements the Rayleigh length and waist radius are approximately $400 \pm 50 \mu\text{m}$ and $9.0 \pm 0.5 \mu\text{m}$, respectively.

and a CEP resolution of ~ 80 mrad, corresponding to ~ 60 attoseconds ($\ll 2.3$ fs, the optical period of light with $\lambda \approx 700$ nm).

In this work we present a quantitative, direct, three-dimensional mapping of the CEP evolution of a focused broadband laser beam, spanning a range of seven times the Rayleigh range along the propagation axis and one and a half times the local beam radius perpendicular to the optical axis. To achieve this, we have combined a nanotip-based focus characterisation setup with a xenon-gas-based, stereographic, above-threshold ionisation (ATI) CEP-meter. Every laser pulse from a hollow-core fibre compressor is split between the two separate, but synchronized and parallel measurements: one for individual characterisation of the random CEP of each shot and the other for recording electron spectra from the laser-nanotip interaction^{26,28}, see Methods and Supplementary information. In this way, every detected electron from the nanotip can be associated with the CEP-value for the specific laser pulse producing that electron. The beam towards the nanotip focus measurement was spatially filtered to remove higher modes and provide a good TEM_{00} approximation as required for the following model. Measurements were done to probe the

relative CEP-shift both along the laser's propagation axis and radially outward, mapping the cylindrically-symmetric three-dimensional space. Both tungsten and gold tips were used. In comparison to previous experimental work²³⁻²⁵, in this measurement we probe the focus of a typical intense few-cycle pulse laser beam with a significantly better spatial resolution, scan a larger range of the focal volume and attain a well-defined focus with minimized aberrations by use of an off-axis parabolic mirror and a spatial filter element upfront. In combination with considerable efforts to flatten the spectral phase, these factors allow for a clear and thorough experimental and theoretical investigation of deviations from the monochromatic Gouy phase and additionally reveal the transverse phase structure.

The longitudinal phase difference for a focused, *continuous* and *monochromatic* Gaussian beam as compared to a plane wave is described along the propagation axis by

$$\Delta\psi(z) = -\arctan\left(\frac{z}{z_R}\right), \quad (1)$$

and is known as the Gouy phase, where z is the laser propagation direction and z_R is the Rayleigh length^{1,6,23}.

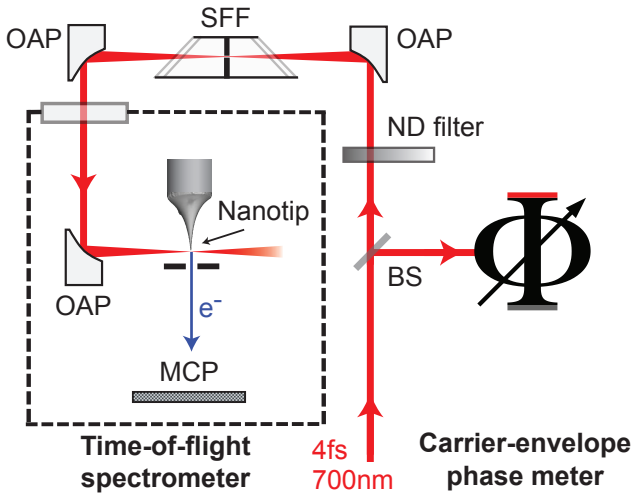


FIG. 2. **Overview of the phase-tagging scheme with a nanotip.** For parallel determination of the laser pulse’s CEP and the time-of-flight of electrons from the nanotip, an amplified 4 fs, 700 nm central wavelength, horizontally polarized pulse train from a laser system with a hollow core fibre compressor is split at the beam splitter (BS) towards the carrier-envelope phase meter arm (right), and the time-of-flight spectrometer arm (left), respectively. The spatial mode of the beam to the nanotip is cleaned with a spatial frequency filter (SFF). The beam is focused inside the ultrahigh vacuum chamber with a 90° off-axis parabolic mirror (OAP, $f = 50$ mm) on the nanotip. The TOF spectrometer records the flight time of photoelectrons with a microchannel-plate (MCP) that is then converted into kinetic energy and provides the x-axis for the spectrum in Fig. S2, see Supplementary information. The CEP-meter measures the randomly varying carrier-envelope phase of each and every shot and thus resolves the spectrum along the y-axis in Fig. S2. For full details see Supplementary information.

Laser *pulses* on the other hand are composed of a coherent superposition of a broad range of wavelengths, leading to a much more complex, spatially-dependent phase profile. Moreover, the transverse shape and the divergence of the Gaussian beam in front of the focusing element are, in general, wavelength dependent. Thus, it is necessary to take into account the wavelength-dependent input beam geometry in order to determine the spatial dependence of the CEP after the focusing element. A more generalized treatment of the strong focusing of chirp-free pulsed Gaussian beams in terms of their properties prior to focusing, combines the concept of enveloped carrier oscillations with fundamental diffraction theory², which introduces iso-carrier-phase fronts and pulse-peak fronts^{5,6}. Their difference results in a relative CEP-shift in the focal area of

$$\Delta\phi(z, r) = -\arctan\left(\frac{z}{z_R}\right) + \frac{g_0 \cdot \left[1 - 2\left(\frac{r}{w(z)}\right)^2\right]}{\frac{z}{z_R} + \frac{z_R}{z}}, \quad (2)$$

where $\Delta\phi$ is defined to be 0 in the focal reference plane (defined by $z = 0$) for all radii r ; here, z_R is the Rayleigh length at the centre frequency; $w(z)$ is the z -dependent beam radius, and $r/w(z)$ is the normalized radial coordinate, see Supplementary information. The last term of Eq. 2 describes the difference to the axial Gouy phase, Eq. 1, and accounts for the wavelength-dependent geometry of the input beam and the difference in curvature of the carrier-phase fronts as compared to that of the pulse fronts. This term scales with g_0 — a dimensionless geometry factor of the input beam evaluated at the central angular frequency of the laser spectrum ω_0 , which we call the Porras factor^{5,6}.

The Porras factor is given by

$$g_0 = \left. \frac{dZ_R(\omega)}{d\omega} \right|_{\omega_0} \cdot \frac{\omega_0}{Z_R(\omega_0)} \quad (3)$$

and represents the normalized first derivative of the *input* beam’s Rayleigh length, $Z_R(\omega)$ (capital letters are used for input beam parameters), with respect to the laser’s spectral angular frequencies, ω , evaluated at ω_0 . The Rayleigh length before the focussing element is linked to the frequency dependent input beam waist, $W(\omega)$, by $Z_R(\omega) = \omega \cdot W(\omega)^2 / (2c)$, where c is the speed of light. Three characteristic cases can be highlighted: (i) $g_0 = -1$ for an isodiverging input beam, i.e. with a constant divergence angle for all ω ; (ii) $g_0 = 0$ for an isodiffracting beam, i.e. with a constant Rayleigh length; and (iii) $g_0 = +1$ for a beam with a frequency independent waist radius⁶ (see Fig. 1 for example phase profiles and Fig. 3 for case $g_0 = 0$). Note that at $g_0 = 0$, all frequencies are diffracted identically in the first order approximation and hence the phase shift consists merely of the Gouy component. However, one ought not simply assume or expect g_0 to be 0 as this is just one special and specific case, which is within a continuous range of possible g_0 values and rarely found in practice.

Figure 3 shows the results of two on-axis measurements together with the monochromatic Gouy phase curve. The measured CEP shows extrema at $z \approx 1.7$ times the Rayleigh length both before and after the focus, resulting in a much steeper slope in the focal plane as compared to the arctangent-curve of the Gouy phase. The data can be fitted well by Eq. 2 at $r = 0$, resulting in $g_0 = -2.1 \pm 0.2$ for the first (I) and -1.8 ± 0.3 for the second (II) dataset. These g_0 -values are corroborated by independent measurements of the spectral input beam properties outside the vacuum chamber, namely the spectrally resolved Rayleigh length calculated from the beam diameter. This provides an attractive and more easily attainable alternative way to estimate g_0 via Eq. 3 and, therefore, obtain an approximate idea of the focal CEP

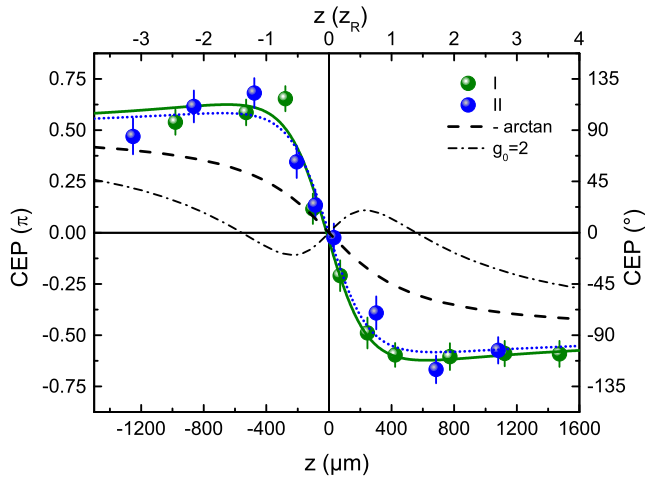


FIG. 3. **On-axis carrier-envelope phase.** CEP as a function of propagation distance, z , on the optical axis. Two traces have been recorded, data set I (green spheres, Rayleigh length $z_R = 380 \pm 50 \mu\text{m}$) and II (blue spheres, $z_R = 365 \pm 50 \mu\text{m}$). The error bars show the measurement uncertainties in CEP of $\approx 0.2\text{rad}$, as described in the Supplementary information. The experimental data points were fitted by a theoretical model (Eq. 2 solid green and dotted blue curves), yielding fitting parameters of $g_0 = -2.1 \pm 0.2$ (reduced $\chi^2 = 1.3$) for data set I and $g_0 = -1.8 \pm 0.3$ (reduced $\chi^2 = 1.6$) for data set II. For comparison, we show the monochromatic Gouy phase, corresponding to the case $g_0 = 0$, for a Rayleigh length of $z_R = 400 \mu\text{m}$ (black dashed curve), which is clearly unable to explain our observations. The dashed-dotted line depicts the theoretical curve for $g_0 = +2$ and $z_R = 400 \mu\text{m}$, as an example phase behaviour for another beam geometry (lineout of Fig. 1 d). Data sets I and II have been recorded with different tip materials, see Supplementary information.

evolution in the interaction region, see Supplementary information and Fig. 1. Note that further work is warranted and needs to determine whether this technique will fulfill its promise. In addition, the similarity of the experimental curves in Fig. 3 shows the reproducibility of the measurement.

We were also able to produce a three-dimensional map of the CEP by scanning both z and r with the tip (Fig. 4). We observe that there is a strong radial dependence of the CEP, again differing from the monochromatic Gouy phase. Fitting Eq. 2 to the data points yields $g_0 = -1.2 \pm 0.3$, where g_0 and the offsets in z, r and $\Delta\phi$ are free parameters and the Rayleigh length z_R was determined independently by a knife-edge measurement to $z_R = 350 \pm 50 \mu\text{m}$, see Supplementary information. For negative g_0 values, as observed in all measurements here, characteristic features of the CEP around the focus can be recognized, see Figs. 4 and 1: (i) The radial dependence of the CEP surface is concave before, e.g. at $z = -800 \mu\text{m}$, and convex after the focus, e.g. at $z = 800 \mu\text{m}$. (ii) Radially further out from the axis, i.e. $r \gtrsim w(z)$, the CEP changes sign, implying that the vector

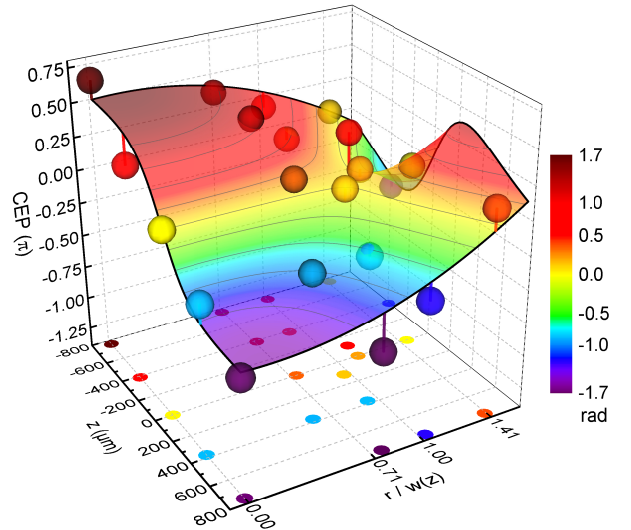


FIG. 4. **Off-axis carrier-envelope phase evolution.** Three-dimensional plot of the CEP as a function of propagation distance z and normalized radial coordinate $r/w(z)$. The experimental data points are depicted by colour-coded spheres whose size encompasses their uncertainty resulting from measurement errors in positioning and determination of the CEP ($\approx 0.2\text{rad}$), as described in the Supplementary information. To further clarify the z - r -position of the measured data, each data point is projected in the z - r -plane. A surface defined by Eq. (2) was fit to the data (coloured), yielding a fit parameter of $g_0 = -1.2 \pm 0.3$ (reduced $\chi^2 = 3.7$). See also Fig. 1b for a plot with a similar g_0 and Supplementary information for a stereoscopic view and a projected contour plot. The Rayleigh length is $350 \pm 50 \mu\text{m}$, independently determined with a knife-edge measurement.

potential at the pulse peak changes sign as well (see Supplementary Eq. 9). In other words, the CEP evolves with opposite slopes on and off the optical axis. And (iii) in the focal plane at the waist radius, i.e. at $(z, r) = (0, w_0)$, the phase exhibits a saddle point. In this measurement, the value for g_0 differs from that obtained previously in the on-axis case as it was done with different laser tuning. This underscores the need to properly characterise the light source in use and determine the influence of laser tuning parameters, such as hollow-core fibre pressure, on the spectral geometry of the output beam and g_0 in order to facilitate advanced phase control in the future.

In the present experiment, the nanotip samples such a small volume of the laser focus in comparison to the Rayleigh range and the focal waist size that it can be assumed that only a single intensity and phase are effective. However, this is not the case in most ultrafast, laser-induced processes. To account for the fact that common targets often experience a large range of laser intensities, one must properly weight the results with the intensity and target-density profiles, i.e. the intensity-volume effect needs to be taken into account²⁹. Further, here we see that this problem is significantly exacerbated for

broadband lasers as there is an analogous and coupled phase-volume effect due to the two-dimensional phase profile. In some situations, these complications could be reduced by physically limiting the extent of the target or effectively limiting it by selecting a high-order process. However, they are by no means eliminated. For example, even for a target, very thin in the laser-propagation direction, $\Delta z \ll z_R$, the phase is often strongly radially dependent even within the beam width. Thus, the common assumption of an arctangent dependence of the CEP is often unwarranted and insufficient.

Although these effects can complicate interpretation, they also have the potential to be used to enhance desired effects and perhaps even be utilized in novel ways, for

instance, to improve phase matching in high-order harmonic (HHG) and attosecond pulse generation. Further, one could optimize these effects by tailoring the interaction region via the input beam geometry, expressed by g_0 . In addition, we expect that recent developments such as particle trapping and acceleration of atoms with femtosecond laser pulses may benefit from the CEP control demonstrated here through an interesting well-like structure formed by the CEP-gradients^{30–32}. Hence, new ways of controlling atoms with large forces through ultrashort, strong laser fields may result. The detailed knowledge of the phase evolution found here impacts many fields where knowledge and control of the optical phase is vital and fascinating developments can be foreseen.

* These authors contributed equally to this work.

- ¹ Gouy, L. G. Sur une propriété nouvelle des ondes lumineuses. *C. R. Acad. Sci. Paris* **110**, 1251–1253 (1890).
- ² Born, M. & Wolf, E. *Principles of optics: electromagnetic theory of propagation, interference and diffraction of light* (Cambridge University Press, 1999).
- ³ Siegman, A. E. *Lasers*, vol. 37 (University Science Books, Mill Valley, CA, 1986).
- ⁴ Visser, T. & Wolf, E. The origin of the Gouy phase anomaly and its generalization to astigmatic wavefields. *Opt. Commun.* **283**, 3371–3375 (2010).
- ⁵ Porras, M. A. Diffraction effects in few-cycle optical pulses. *Phys. Rev. E* **65**, 026606 (2002).
- ⁶ Porras, M. A. Characterization of the electric field of focused pulsed Gaussian beams for phase-sensitive interactions with matter. *Opt. Lett.* **34**, 1546–1548 (2009).
- ⁷ Krüger, M., Schenk, M. & Hommelhoff, P. Attosecond control of electrons emitted from a nanoscale metal tip. *Nature* **475**, 78–81 (2011).
- ⁸ Wachter, G. *et al.* Electron rescattering at metal nanotips induced by ultrashort laser pulses. *Phys. Rev. B* **86**, 035402 (2012).
- ⁹ Piglosiewicz, B. *et al.* Carrier-envelope phase effects on the strong-field photoemission of electrons from metallic nanostructures. *Nat. Photon.* **8**, 37–42 (2014).
- ¹⁰ Gordon, R. J. & Barge, V. J. Effect of the Gouy phase on the coherent phase control of chemical reactions. *J. Chem. Phys.* **127**, 204302 (2007).
- ¹¹ Johnson, J. L., Dorney, T. D. & Mittleman, D. M. Enhanced depth resolution in terahertz imaging using phase-shift interferometry. *Applied Physics Letters* **78**, 835–837 (2001).
- ¹² Drexler, W. & Fujimoto, J. G. *Optical coherence tomography: technology and applications* (Springer Science & Business Media, 2008).
- ¹³ Krausz, F. & Stockman, M. I. Attosecond metrology: from electron capture to future signal processing. *Nat. Photon.* **8**, 205–213 (2014).
- ¹⁴ Udem, T., Holzwarth, R. & Hänsch, T. W. Optical frequency metrology. *Nature* **416**, 233–237 (2002).
- ¹⁵ Kling, M. *et al.* Control of electron localization in molecular dissociation. *Science* **312**, 246–248 (2006).
- ¹⁶ Baltuška, A. *et al.* Attosecond control of electronic processes by intense light fields. *Nature* **421**, 611–615 (2003).
- ¹⁷ Zhrebtsov, S. *et al.* Controlled near-field enhanced electron acceleration from dielectric nanospheres with intense few-cycle laser fields. *Nat. Phys.* **7**, 656–662 (2011).
- ¹⁸ Fordell, T., Miranda, M., Arnold, C. & L’Huillier, A. High-speed carrier-envelope phase drift detection of amplified laser pulses. *Opt. Express* **19**, 23652–23657 (2011).
- ¹⁹ Paasch-Colberg, T. *et al.* Solid-state light-phase detector. *Nat. Photon.* **8**, 214–218 (2014).
- ²⁰ Goulielmakis, E. *et al.* Attosecond control and measurement: Lightwave electronics. *Science* **317**, 769–775 (2007).
- ²¹ Shverdin, M., Walker, D., Yavuz, D., Yin, G.-Y. & Harris, S. E. Generation of a single-cycle optical pulse. *Phys. Rev. Lett.* **94**, 033904 (2005).
- ²² Wirth, A. *et al.* Synthesized light transients. *Science* **334**, 195–200 (2011).
- ²³ Lindner, F. *et al.* Gouy phase shift for few-cycle laser pulses. *Phys. Rev. Lett.* **92**, 113001 (2004).
- ²⁴ Tritschler, T., Hof, K., Klein, M. & Wegener, M. Variation of the carrier-envelope phase of few-cycle laser pulses owing to the Gouy phase: a solid-state-based measurement. *Opt. Lett.* **30**, 753–755 (2005).
- ²⁵ Major, B., Nemes, D., Porras, M. A., Horváth, Z. L. & Kovács, A. P. Carrier-envelope phase changes in the focal region: propagation effects measured by spectral interferometry. *Applied Optics* **54**, 10717–10724 (2015).
- ²⁶ Wittmann, T. *et al.* Single-shot carrier-envelope phase measurement of few-cycle laser pulses. *Nat. Phys.* **5**, 357–362 (2009).
- ²⁷ Thomas, S., Krüger, M., Förster, M., Schenk, M. & Hommelhoff, P. Probing of optical near-fields by electron rescattering on the 1 nm scale. *Nano Lett.* **13**, 4790–4794 (2013).
- ²⁸ Johnson, N. G. *et al.* Single-shot carrier-envelope-phase-tagged ion-momentum imaging of nonsequential double ionization of argon in intense 4-fs laser fields. *Phys. Rev. A* **83**, 013412 (2011).
- ²⁹ Sayler, A., Wang, P., Carnes, K. & Ben-Itzhak, I. Determining intensity dependence of ultrashort laser processes through focus z-scanning intensity-difference spectra: application to laser-induced dissociation of H₂⁺. *J. Phys. B: At. Mol. Opt. Phys.* **40**, 4367–4378 (2007).
- ³⁰ Shane, J. C., Mazilu, M., Lee, W. M. & Dholakia, K. Effect of pulse temporal shape on optical trapping and impulse transfer using ultrashort pulsed lasers. *Opt. Express* **18**, 7554–7568 (2010).

- ³¹ Freearge, T., Walz, J. & Hänsch, T. Confinement and manipulation of atoms using short laser pulses. *Opt. Commun.* **117**, 262–267 (1995).
- ³² Eichmann, U., Nubbemeyer, T., Rottke, H. & Sandner, W. Acceleration of neutral atoms in strong short-pulse laser fields. *Nature* **461**, 1261–1264 (2009).

ACKNOWLEDGEMENTS

We gratefully acknowledge Michael Förster for supplying nanotips, and Peter Dombi and Sebastian Thomas for support in the measurement campaign. This work has been supported by the DFG Grant PA 730/5, Laserlab-Europe EU-H2020 654148, ERC Grant NearFieldAtto, DFG Cluster of Excellence Munich Center for Advanced Photonics. D.H. acknowledges the Helmholtz Association for financial support. M.K. acknowledges the Minerva Foundation and the Koshland Foundation for financial support.

AUTHOR CONTRIBUTIONS

All authors contributed to all parts of the experiment including the final version of the manuscript.

METHODS

We employ a phase-tagging method²⁸ for recording the CEP-dependent electron back-scattering at tungsten and gold nanotips, placed at different points near the focus (see Figs. S1 and S2 in the Supplementary information). This method utilizes simultaneous measurements of electron time-of-flight spectra from the metal nanotip in event-mode on the one hand, and of the CEP of every single shot of the few-cycle pulse train on the other, the latter being determined by a phasemeter²⁶. The events in both measurements are synchronized by triggering on the same laser pulse. Both measurements rely upon the strong CEP dependence of backscattered, laser driven photo-electrons, i.e. those electrons that return to their parent matter and scatter elastically back from it after acceleration in the optical field.

In the CEP-meter the two electron spectra that build up from xenon in the left and right direction of the horizontal laser polarization are recorded and compared by calculating the asymmetry parameter $A = \frac{N_L - N_R}{N_L + N_R}$, i.e. the contrast, where N is the electron yield left and right, respectively. From this parameter the CEP of the laser shot can be evaluated²⁶. Exploiting the high spatial resolution and pronounced CEP sensitivity of the electron backscattering at the metal nanotip, we recorded phase-tagged kinetic-energy spectra at positions on the optical axis and off-axis on hyperbolic curves in a plane along the focus (see Fig. 1 and S2 in the Supplementary information).